Digest Journal of Nanomaterials and Biostructures Vol. 15, No. 2, April - June 2020, p. 545 - 553

PHOTODEPOSITION SYNTHESIS AND CHARACTERIZATION OF Ag/ZnO NANOCOMPOSITES FOR PHOTODEGRADATION OF METHYLENE BLUE AND METHYL ORANGE

S. BUAPOON[a], A. PHURUANGRAT[a,*], T. THONGTEM[b,c], S. THONGTEM[c,d]
[a]*Department of Materials Science and Technology, Faculty of Science, Prince of Songkla University, Hat Yai, Songkhla 90112, Thailand*
[b]*Department of Chemistry, Faculty of Science, Chiang Mai University, Chiang Mai 50200, Thailand*
[c]*Materials Science Research Center, Faculty of Science, Chiang Mai University, Chiang Mai 50200, Thailand*
[d]*Department of Physics and Materials Science, Faculty of Science, Chiang Mai University, Chiang Mai 50200, Thailand*

In this work, Ag nanoparticles were deposited on hierarchical ZnO nanostructure flowers by photodeposition method. The as-prepared samples were characterized by X-ray diffraction (XRD), field emission scanning electron microscopy (FE-SEM) coupled with energy dispersive spectrometer (EDS), Fourier transform infrared (FTIR) spectrometry and X-ray photoelectron spectroscopy (XPS). Photocatalytic performance of the as-prepared ZnO and Ag/ZnO nanocomposites was investigated through photodegradation of methylene blue (MB) and methyl orange (MO) as cationic and anionic dye models under UV light irradiation. The analytical results showed that the spherical metallic Ag nanoparticles with 10–12 nm diameter were deposited on nanosheets as petals of hierarchical ZnO nanostructure flowers. The photodegradation efficiencies of MB and MO by Ag/ZnO nanocomposites were higher than that by pure ZnO sample because of the electronic transfer through Ag/ZnO heterojunctions.

(Received February 7, 2020; Accepted June 2, 2020)

Keywords: Photodeposition; Ag/ZnO nanocomposites; Photocatalysis

1. Introduction

Semiconductor-based photocatalysts have attracted much attention in recent years due to their potential applications in environmental purification and solar energy transformation [1-7]. Semiconductor-based photocatalysts such as TiO_2 [1, 2], ZnO [3, 4], MoO_3 [5], Bi_2MoO_6 [6] and $ZnFe_2O_4$ [7] have been widely used for photodegradation of dye pollutant in wastewater because of their surface reactions generate reactive oxygen species such as hydroxyl radical, superoxide anion radical and H_2O_2 which are responsible for degradation of pollutant in wastewater [8]. Among them, ZnO with a wide band gap of 3.37 eV and large exciton binding energy of 60 meV at room temperature is a promising material used for degrading of organic dyes because it has high electron mobility, diversified morphologies, low cost, high chemical stability and environmental friendly [3, 4, 8-11]. Nevertheless, photocatalytic activity of ZnO is low because it has very fast recombination rate of photogenerated charge carriers [8-12]. Different methods such as doping materials [3, 8], composites [12-14] and surface modification [15, 16] have been adopted to reduce recombination rate of photogenerated charge carriers of ZnO in order to increase its photocatalytic activity [3, 8, 12-17]. Photocatalytic activity of ZnO can be enhanced through its hybridization with noble metals such as Pt, Ag, Au and Pd to prolong the lifetime of photogenerated charge carriers [9, 10, 12-14, 17]. For example, Chen et al. succeeded in synthesizing of Au/ZnO microstructure flowers through an aqueous solution route [12]. The composites showed photocatalytic activity higher than pure ZnO sample. Saidani et al. reported the

* Corresponding author: phuruangrat@hotmail.com

synthesis of nanocrystalline Ag/ZnO powder by a modified polyol process using triethylene glycol solvent as a reducing and stabilizing agent [13]. Ag/ZnO photocatalysts with optimized x = 0.7% Ag showed 14 times rate of degradation of diuron higher than that of unmodified ZnO sample. Mauro et al. succeeded in synthesizing of ZnO nanofibers mixed with Pt nanoparticles by pulsed laser ablation in liquid used for photodegradation of methylene blue (MB) under UV light irradiation [14]. Comparing to other noble metals, Ag is more widespread owing to its high electrical and thermal conductivity, low cost, nontoxicity and antibacterial properties [9, 10, 13]. Thus, heterogeneous Ag/ZnO nanocomposites can be used for photocatalytic degradation of organic dyes.

In this research, heterogeneous Ag/ZnO nanocomposites were synthesized by photodeposition process. Photodeposition is a facile, efficient flexible and versatile process, which is an alternative process for synthesizing of other heterogeneous photocatalysts. The photocatalytic properties of heterogeneous Ag/ZnO nanocomposites used for the degradation of methyl blue (MB) and methyl orange (MO) dye models under UV light irradiation were studied and discussed.

2. Experiment

Flower-like ZnO samples were prepared by direct precipitation method. 13.3866 g $Zn(NO_3)_2 \cdot 6H_2O$ was dissolved in 200 ml reverse osmosis (R.O.) water under continued stirring. Subsequently, 40 ml of 3 M NaOH solution was added to Zn^{2+} solution under vigorous stirring for 24 h to form white precipitates, which were filtered, washed and dried. Subsequently, the precipitates were calcined at 600 ^oC by 5 ^oC min^{-1} heating rate for 2 h in ambient atmosphere.

To prepare Ag/ZnO nanocomposites, different contents of $AgNO_3$ for 1%, 5% and 10% by weight of Ag were dissolved in 100 ml ethylene glycol containing 2.5 g ZnO suspension under constant stirring for 30 min. Then, they were irradiated by UV light for 3 h. The as-prepared precipitates were collected, washed with deionized water and dried for further characterization.

The crystallinity and crystalline phase of the synthesized samples were analyzed by X-ray diffraction (XRD, Philips X'Pert MPD) with Cu K_α radiation as an X-ray source in the range of 20^o–60^o. The structural investigation was carried out by a field emission scanning electron microscope (FE-SEM, JEOL JSM-6335F) at an acceleration voltage of 20 kV coupled with an Oxford INCA energy dispersive spectrometer (EDS). A Fourier transform infrared (FTIR) spectrometer was carried out through a Bruker Tensor 27 spectrometer at room temperature in the range of 400–4000 cm^{-1}. Pellets of ZnO samples were prepared by 40 times KBr dilution for FTIR testing. X-ray photoelectron spectroscopy (XPS) was carried out using an Axis Ultra DLD | Kratos - Kratos Analytical with a monochromated Al K_α radiation (1486.6 eV) as a providing source. All XPS spectra were calibrated with respect to a C 1s electron peak at 285.1 eV.

MB and MO as cationic and anionic dye models were used to test for photocatalytic activities of ZnO containing different contents of Ag at room temperature under UV light irradiation. The reaction was carried out through the solution of 200 mg catalyst dispersed in 200 ml of 1 x 10^{-5} M dye aqueous solution. Prior to irradiation, the suspension was magnetically stirred in the dark for 30 min to establish an adsorption/desorption equilibrium of the dye and the catalyst. During testing, approximately 5 ml samples were withdrawn every 30 min. The aqueous solution was centrifuged to remove any suspended solid particle. The residual concentration of dye was measured at 664 nm for MB solution and 465 nm for MO solution containing in a microcuvette using R.O. water as a reference by a UV-visible spectrophotometer (Perkin–Elmer Lambda 25). The degradation efficiency was calculated by the equation given below.

$$\text{Decolorization efficiency (\%)} = \frac{C_o - C_t}{C_o} \text{x}100 \quad (1)$$

C_o is the initial dye concentration and C_t is the dye concentration after testing for a period of time (t).

3. Results and discussion

Fig. 1 shows XRD patterns of as-synthesized ZnO and heterostructure Ag/ZnO samples. The observed XRD pattern of pure ZnO sample can be well indexed to the (100), (002), (101), (102) and (110) planes of hexagonal wurtzite ZnO structure according to JCPDS no. 36-1451 [18]. The as-prepared heterostructure Ag/ZnO samples show new diffraction peaks at $2\Theta = 38.21^{o}$ and 44.41^{o} which can be indexed to the (111) and (200) planes of face-centered cubic (FCC) Ag according to JCPDS no. 04-0783 [18]. Clearly, Ag nanoparticles formed by photoreduction on the surface of hexagonal ZnO nanostructure. Impurities were not detected in all samples. The results certified that the as-synthesized products were pure wurtzite ZnO phase for ZnO sample and mixed phases of wurtzite ZnO as major phase and FCC Ag phase as minor phase for heterostructure Ag/ZnO samples. According to Scherrer equation [1, 3, 16], the average crystallite size of FCC Ag nanoparticles from (111) plane in 10% Ag/ZnO sample was estimated to be 32.75 nm.

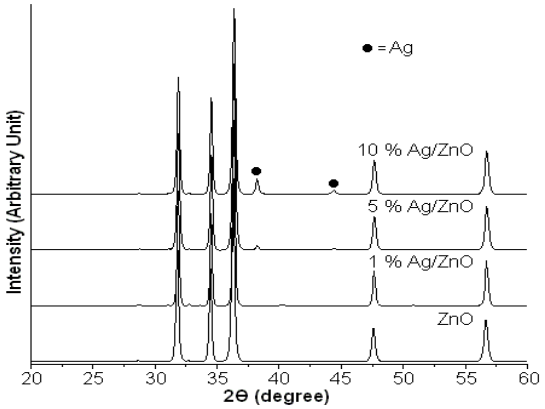

Fig. 1. XRD patterns of 0–10% Ag/ZnO nanocomposites prepared by photodeposition method.

Fig. 2 shows FTIR spectra of pure ZnO and heterostructure Ag/ZnO nanocomposites in wavenumber range of 400–4000 cm^{-1}. Pure ZnO and heterostructure Ag/ZnO nanocomposites show FTIR peak at 440 cm^{-1} attributed to the Zn–O stretching vibration mode [15, 19, 20]. The broad band at 3050–3665 cm^{-1} of the samples corresponds to O–H bonding of adsorbed water on surface of the samples [15, 19, 20].

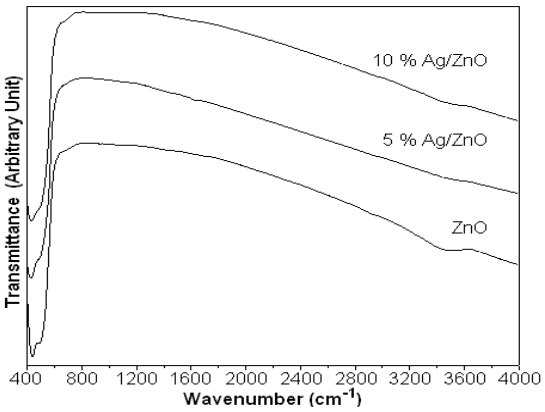

Fig. 2. FTIR spectra of 0–10% Ag/ZnO nanocomposites prepared by photodeposition method.

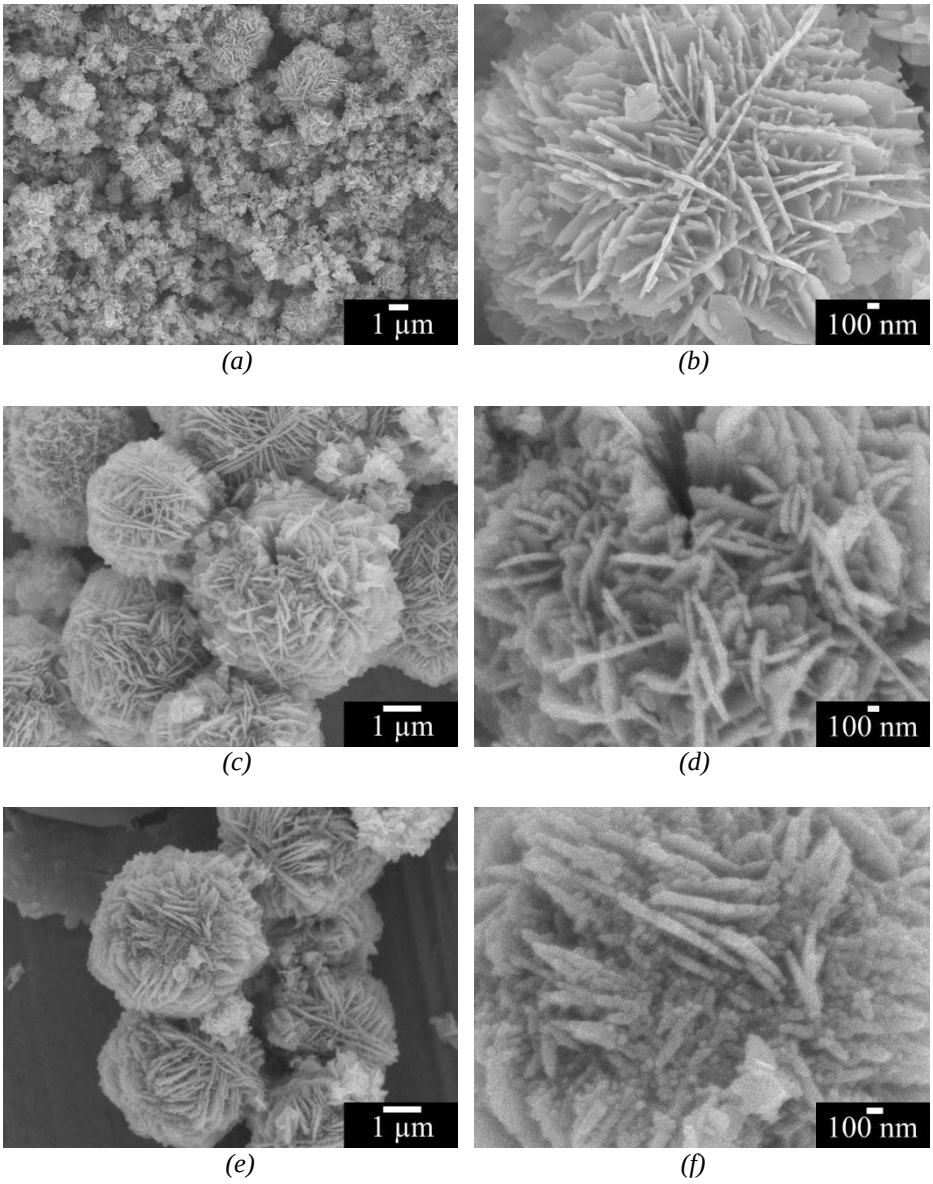

Fig. 3. SEM images at low and high magnifications of (a, b) ZnO, (c, d) 5% Ag/ZnO and (e, f) 10% Ag/ZnO nanosamples prepared by photodeposition method.

Fig. 3a and b shows SEM images of the hierarchical flower-like ZnO nanostructure. Clearly, pure ZnO sample was composed of uniform hierarchical ZnO flowers with 2–4 μm in diameter. The flowers were the assemblies of nanosheets as petals with smooth surfaces. They should be noted that all nanosheets grew out of spherical cores. This phenomenon can be explained by the rule of evolutionary selection for crystal growth in a limited space [21]. Geometrically, the inner part of a solid sphere is considered as an occupied space. Its free outer space is to be occupied. Thus, the nanosheets survive and grow in the direction pointing out of the inner core to outer surface of the sphere. The results can lead to the formation of densely arranged nanosheets standing on the surface of the sphere [21]. The morphologies of 5% and 10% Ag/ZnO nanocomposites at low and high magnifications of Fig. 3c–f show that Ag nanoparticles with 10–12 nm diameter were randomly distributed on the surface of each petal of the hierarchical ZnO flowers. There was no detection of agglomerated Ag nanoparticles, which were randomly dispersed on the surface of ZnO. Furthermore, Ag nanoparticles with the increment of Ag content were deposited on the surface of hierarchical ZnO nanostructure flowers. EDS mapping of 10% Ag/ZnO nanocomposites (Fig. 4) shows elemental mapping of silver, zinc and oxygen from Ag L_{α},

Zn $K_{\alpha 1,2}$ and O $K_{\alpha 1,2}$, respectively. The results indicate that 10% Ag/ZnO nanocomposites were composed of metallic Ag nanoparticles on the surface of hierarchical ZnO nanostructure flowers.

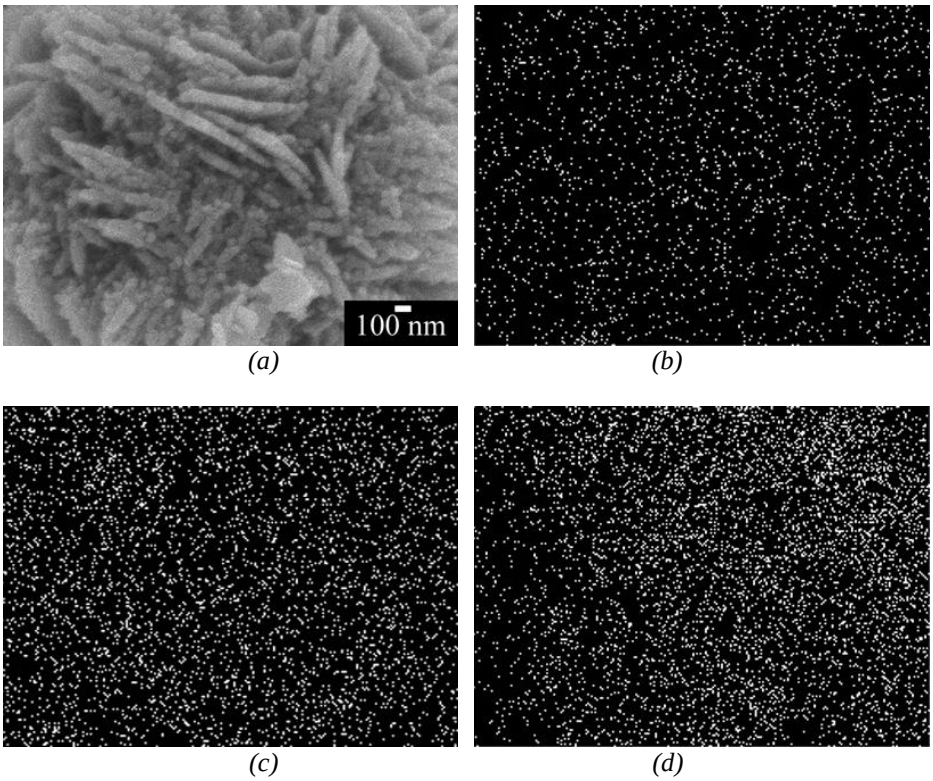

Fig. 4. (a) SEM image and (b–d) EDS mapping of Ag, Zn and O of 10% Ag/ZnO nanocomposites prepared by photodeposition method.

The full survey XPS spectrum of 10% Ag/ZnO nanocomposites (Fig. 5a) using C 1s as a standard presents Ag, Zn and O containing in the sample. No impurities were detected. The high resolution binding energies of Ag 3d (Fig. 5b) were detected at 373.42 eV for Ag $3d_{3/2}$ and 367.42 eV for Ag $3d_{5/2}$ which were specified as the oxidation state of Ag^0 containing in the composites [10, 22, 23]. Comparing with bulk metallic Ag with binding energies of Ag $3d_{3/2}$ at 374. 2 eV and Ag $3d_{5/2}$ at 368.2 eV [23, 24], binding energies of Ag 3d containing in 10% Ag/ZnO nanocomposites were lessened because their Fermi levels were adjusted upon contact [25, 26]. Fig. 5c is the high resolution spectrum of Zn $2p_{3/2}$ and Zn $2p_{1/2}$ core levels which were detected energy peaks at 1021.27 eV and 1044.36 eV. The results indicated that Zn^{2+} ions contained in wurtzite ZnO flowers [8, 10, 25, 26]. The deconvoluted high resolution spectrum of O 1*s* (Fig. 5d) shows four Gaussian peaks at 530.17 eV, 531.29 eV, 532.11 eV and 533.25 eV which are assigned to Zn–O bonding in hexagonal wurtzite ZnO structure, oxygen vacancies and adsorbed H_2O and CO_2 on the surface of ZnO [8, 22, 24, 25].

Photocatalytic performances of the as-prepared ZnO nanostructure flowers and Ag/ZnO nanocomposites were evaluated through the photodegradation of MB and MO as organic dyes under UV light irradiation. Fig. 6 shows UV-visible absorption spectra of MB and MO solutions over 10% Ag/ZnO nanocomposites under UV light irradiation within different duration of time. The characteristic absorption peaks of MB at 664 nm and MO at 465 nm were decreased with increasing in the UV exposure time. At the end of 300 min, MB was degraded faster than MO. The results certified that MB cationic dye absorbed on the surface of ZnO is better than MO anionic dye.

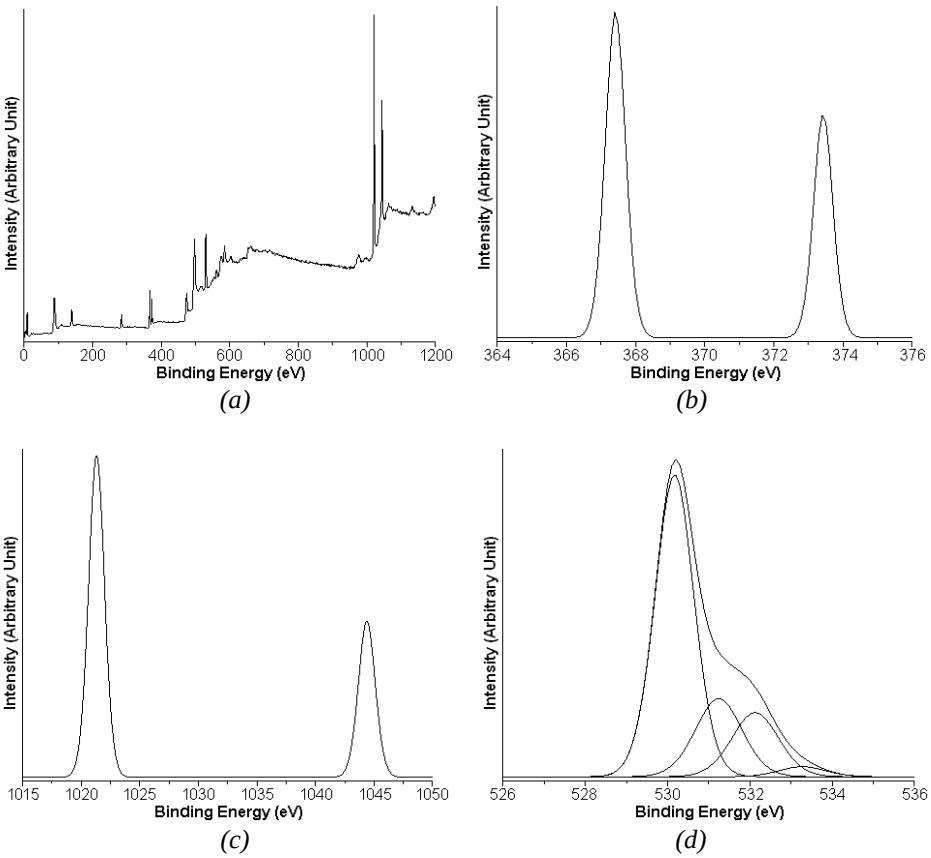

Fig. 5. (a) XPS survey spectrum and (b–d) high resolution spectra of Ag 3d, Zn 2p and O 1s of 10% Ag/ZnO nanocomposites.

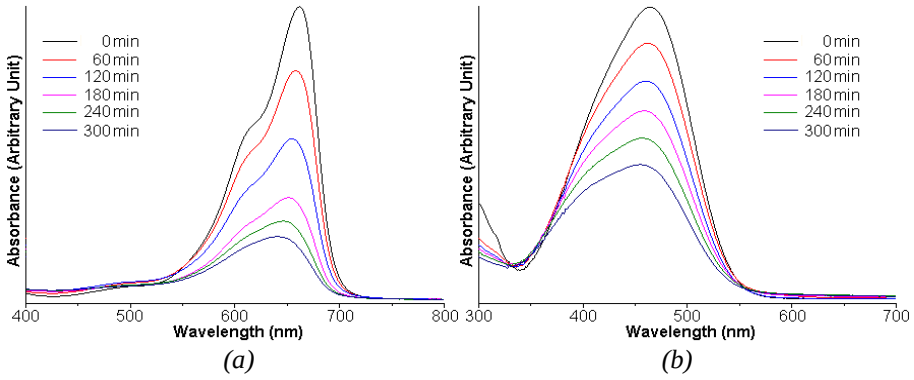

Fig. 6. UV-visible spectra for photodegradation of (a) MB and (b) MO by 10% Ag/ZnO nanocomposites under UV light irradiation.

The photocatalytic degradation of MB and MO by the as-prepared ZnO nanostructure flowers and Ag/ZnO nanocomposites under UV light irradiation is shown in Fig. 7. It can be seen that the photocatalytic efficiency of as-prepared ZnO flowers used for degradation of MB and MO was increased with increasing in the content of Ag. The photocatalytic efficiencies for degradation of MB and MO are in sequence as follows: ZnO < 1% Ag/ZnO < 5% Ag/ZnO < 10% Ag/ZnO. The photocatalytic efficiencies of ZnO, 1% Ag/ZnO, 5% Ag/ZnO and 10% Ag/ZnO samples were 37.47%, 66.99%, 76.29% and 83.78% in degrading of MB and 23.13%, 48.91%, 53.91% and 55.23% in degrading of MO under UV light irradiation within 300 min, respectively. They can be seen that the photodegradation efficiencies of MB and MO over 10% Ag/ZnO nanocomposites are

2.24 and 2.39 times of those of MB and MO over pure ZnO nanostructure flowers. These indicate that Ag nanoparticles loaded on surface of ZnO flowers played the role in improving the photocatalytic efficiency of ZnO sample under UV light irradiation. The photodegradation of ZnO and Ag/ZnO photocatalysts was investigated as the pseudo-first-order plots shown in Fig. 8. The linear plots between the $\ln(C_0/C_t)$ and UV light irradiation for photodegradation of MB and MO over photocatalysts indicate that the photocatalytic degradation of MB and MO over photocatalysts is a pseudo-first-order kinetic model [4, 6, 11]. The pseudo-first-order kinetic constants for MB degradation over photocatalysts were $1.67\text{x}10^{-3}$, $3.61\text{x}10^{-3}$, $4.53\text{x}10^{-3}$ and $6.14\text{x}10^{-3}$ min^{-1} for ZnO, 1% Ag/ZnO, 5% Ag/ZnO and 10% Ag/ZnO samples while the pseudo-first-order kinetic constants for MO degradation were $8.48\text{x}10^{-4}$, $2.06\text{x}10^{-3}$, $2.45\text{x}10^{-3}$ and $2.59\text{x}10^{-3}$ min^{-1} for ZnO, 1% Ag/ZnO, 5% Ag/ZnO and 10% Ag/ZnO samples, respectively. In conclusion, the photocatalytic performance of 10% Ag/ZnO shows the highest photocatalytic performance which is mainly attributed to decrease the recombination of electrons and holes [6, 9, 10, 12, 13].

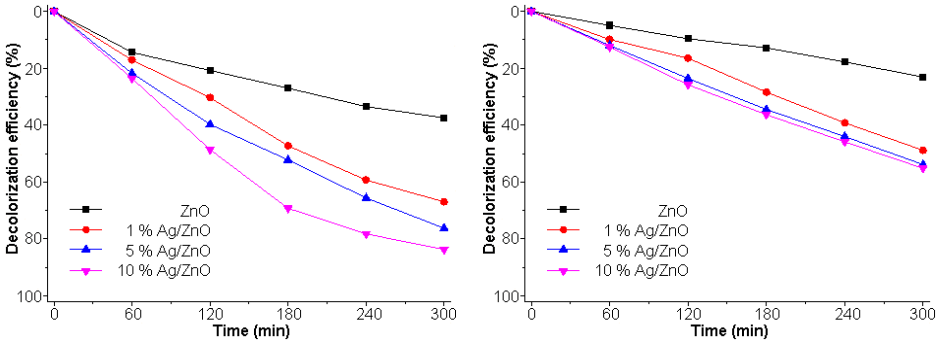

Fig. 7. Decolorization efficiencies of (a) MB and (b) MO by ZnO samples containing different contents of Ag under UV light irradiation.

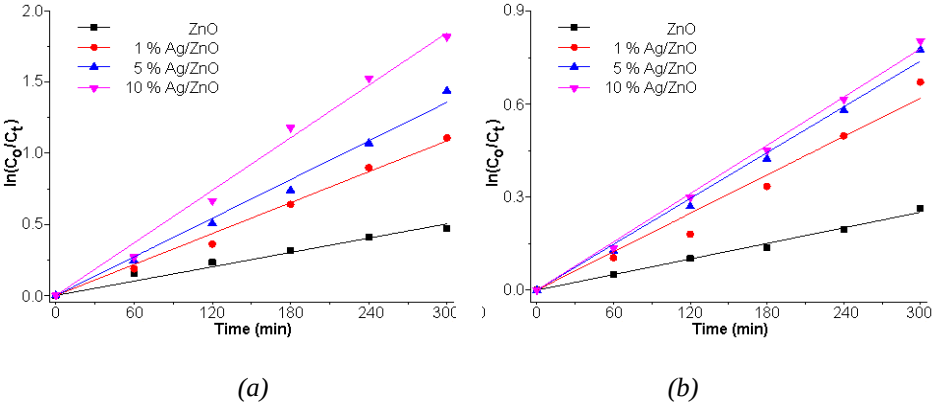

Fig. 8. Pseudo-first-order plots for photodegradation of (a) MB and (b) MO by ZnO containing different contents of Ag under UV light irradiation.

The enhanced photocatalytic activity of Ag/ZnO nanocomposites was controlled by the charge transfer process at the interface between Ag nanoparticles and hierarchical ZnO nanostructure flowers. The as-formed interface can lead to inhibit the recombination of photogenerated charge pairs and to increase the photocatalytic performance of ZnO [9, 10, 13, 27]. Upon UV irradiation, photo-excited electrons and photo-induced holes were generated on conduction band and valence band of ZnO. The conduction band edge of ZnO is under a new equilibrium Fermi level of Ag. Thus the photo-excited electrons and photo-induced holes transferred to Ag nanoparticles and the separation efficiency of photogenerated charge pairs was

enhanced [4, 9, 10, 12, 13, 27]. Subsequently, the photo-induced holes reacted with H_2O/OH^- to form $^{\bullet}OH$ radical and the photogenerated electrons reacted with O_2 to form $^{\bullet}O_2^-$ radical [8, 10, 11, 13, 27]. Ag nanoparticles acted as an acceptor for photo-excited electrons from conduction band of ZnO and promote fast charge transportation because Ag nanoparticles are good electrical conductor [9]. Importantly, Ag nanoparticles supported on ZnO petals led to efficient electron transfer at the interface [9, 10, 13, 27]. The recombination of photogenerated charge pairs was significantly suppressed and the photocatalytic activity of Ag/ZnO nanocomposites was greatly improved [9, 10, 13, 27].

4. Conclusions

In summary, photodeposition method was applied for preparation of heterostructure Ag/ZnO nanocomposites as UV-light-driven photodegradation for MB and MO. The phase, morphologies and oxidation state of element of as-prepared samples were investigated by different techniques including XRD, SEM, EDS, XPS and FTIR. In this research, photodegradation of MB and MO over 10% Ag/ZnO nanocomposites were 2.24 and 2.39 times of that of MB and MO over pure ZnO nanostructure flowers under UV light irradiation. Metallic Ag nanoparticles acted as electron sinks to scavenge electron in conduction band of ZnO, improved the separation of photogenerated charge pairs and enhanced the photocatalytic activities of heterostructure Ag/ZnO nanocomposites.

Acknowledgements

We are extremely grateful to the Faculty of Science Research Fund, Faculty of Science, Prince of Songkla University, Thailand under contract no. 1-2562-02-014.

References

[1] S. Buddee, C. Suwanchawalit, S. Wongnawa, Dig. J. Nanomater. Bios. **12**, 829 (2017).
[2] I. V. Baklanova, V. N. Krasil'nikov, V. P. Zhukov, O. I. Gyrdasova, L. A. Perelyaeva, L. Yu. Buldakova, M. Yu. Yanchenko, I. R. Shein, Russ. J. Inorg. Chem. **9**, 29 (2014).
[3] S. A. Khan, F. Noreen, S. Kanwal, G. Hussain, Dig. J. Nanomater. Bios. **12**, 877 (2017).
[4] M. Rashad, N. M. Shaalan, M. M., Hafiz, Dig. J. Nanomater. Bios. **10**, 823 (2015).
[5] X. Du, X. Wang, Y. Liu, P. Feng, Ceram. Inter. **45**, 12599 (2019).
[6] P. Nuankaeo, A. Phuruangrat, B. Kuntalue, P. Dumrongrojthanath, T. Thongtem, S. Thongtem, Russ. J. Appl. Chem. **89**, 830 (2016).
[7] B. Xu, T. Ding, Y. Zhang, Y. Wen, Z. Yang, M. Zhang, Mater. Lett. **187**, 123 (2017).
[8] F. Achouri, S. Corbel, L. Balan, K. Mozet, E. Girot, G. Medjahdi, M. B. Said, A. Ghrabi, R. Schneider, Mater. Des. **101**, 309 (2016).
[9] S. Seong, I. S. Park, Y. C. Jung, T. Lee, S. Y. Kim, J. S. Park, J. H. Ko, J. Ahn, Mater. Des. **177**, 107831 (2019).
[10] F. Lu, J. Wang, Z. N. Chang, J. Zeng, Mater. Des. **181**, 108069 (2019).
[11] Y. Bao, C. Wang, J. Z. Ma, Mater. Des. **101**, 7 (2016).
[12] C. Chen, Y. Lu, H. He, K. Wu, Z. Ye, Appl. Phys. A **110**, 47 (2013).
[13] M. A. Saidani, A. Fkiri, L. S. Smiri, J. Inorg. Organomet. Polymer. Mater. **29**, 710 (2019).
[14] A. D. Mauro, M. Zimbone, M. Scuderi, G. Nicotra, M. E. Fragalà, G. Impellizzeri, Nanoscale Res. Lett. **10**, 484 (2015).
[15] R. Y. Hong, J. H. Li, L. L. Chen, D. Q. Liu, H. Z. Li, Y. Zheng, J. Ding, Powder Tech. **189**, 426 (2009).
[16] J. Wang, T. Tsuzuki, L. Sun, X. Wang, J. Am. Ceram. Soc. **92**, 2083 (2009).
[17] H. Liu, J. Feng, W. Jie, J. Mater. Sci.: Mater. Electron. **28**, 16585 (2017).

[18] Powder Diffract. File, JCPDS-ICDD, 12 Campus Bld., Newtown Square, PA 19073-3273, U.S.A. (2001).
[19] A. Phuruangrat, S. Thongtem, T. Thongtem, Mater. Des. **107**, 250 (2016).
[20] A. Phuruangrat, T. Thongtem, S. Satchawan, S. Thongtem, Dig. J. Nanomater. Bios. **13**, 625 (2018).
[21] M. Wang, Q. Luo, S. Hussain, G. Liu, G. Qiao, E. J. Kim, Mater. Sci. Semicond. Process. **100**, 283 (2019).
[22] A. Phuruangrat, S. Putdum, P. Dumrongrojthanath, N. Ekthammathat, S. Thongtem, T. Thongtem, Mater. Sci. Semicond. Process. **34**, 175 (2015).
[23] S. Wang, Z. Han, T. Di, R. Li, S. Liu, Z. Cheng, R. Soc. Open Sci. **6**, 191019 (2019).
[24] A. Phuruangrat, P. Dumrongrojthanath, B. Kuntalue, T. Thongtem, S. Thongtem, Dig. J. Nanomater. Bios. **10**, 371 (2015).
[25] A. Ziashahabi, M. Prato, Z. Dang, R. Poursalehi, N. Naseri, Sci. Rep. **9**, 11839 (2019).
[26] M. F. A. Messih, M. A. Ahmed, A. Soltan, S. S. Anis, J. Phys. Chem. Solid. **135**, 109086 (2019).
[27] S. Mohammadzadeh, M. E. Olya, A. M. Arabi, A. Shariati, M. R. K. Nikou, J. Environ. Sci. **35**, 194 (2015).